Development Length in Planar Channel Flows of Newtonian Fluids Under the Influence of Wall Slip

L. L. Ferrás[1]
Institute for Polymers and Composites/I3N,
University of Minho,
Campus de Azurém,
4800-058 Guimarães, Portugal
e-mail: luis.ferras@dep.uminho.pt

A. M. Afonso
e-mail: aafonso@fe.up.pt

M. A. Alves
e-mail: mmalves@fe.up.pt

Departamento de Engenharia Química,
Centro de Estudos de Fenómenos de Transporte,
Faculdade de Engenharia da Universidade do Porto,
Rua Dr. Roberto Frias s/n,
4200-465 Porto, Portugal

J. M. Nóbrega
Institute for Polymers and Composites/I3N,
University of Minho,
Campus de Azurém,
4800-058 Guimarães, Portugal
e-mail: mnobrega@dep.uminho.pt

F. T. Pinho
Centro de Estudos de Fenómenos de Transporte,
Faculdade de Engenharia da Universidade do Porto,
Rua Dr. Roberto Frias s/n,
4200-465 Porto, Portugal
e-mail: fpinho@fe.up.pt

This technical brief presents a numerical study regarding the required development length ($\mathcal{L} = L_{fd}/H$) to reach fully developed flow conditions at the entrance of a planar channel for Newtonian fluids under the influence of slip boundary conditions. The linear Navier slip law is used with the dimensionless slip coefficient $\overline{k}_l = k_l(\mu/H)$, varying in the range $0 < \overline{k}_l \leq 1$. The simulations were carried out for low Reynolds number flows in the range $0 < Re \leq 100$, making use of a rigorous mesh refinement with an accuracy error below 1%. The development length is found to be a nonmonotonic function of the slip velocity coefficient, increasing up to $\overline{k}_l \approx 0.1 - 0.4$ (depending on Re) and decreasing for higher $\overline{k}_l$. We present a new nonlinear relationship between $\mathcal{L}$, Re, and $\overline{k}_l$ that can accurately predict the development length for Newtonian fluid flows with slip velocity at the wall for Re of up to 100 and $\overline{k}_l$ up to 1. [DOI: 10.1115/1.4007383]

[1]Corresponding author.

Contributed by the Fluids Engineering Division of ASME for publication in the Journal of Fluids Engineering. Manuscript received May 14, 2012; final manuscript received July 18, 2012; published online September 24, 2012. Assoc. Editor: Ali Beskok.

1 Introduction

The relevance of the development length is well known in engineering. The assumption that the flow is fully developed in regions where it remains under strong influence of the inlet boundary conditions can seriously underestimate the design of flow systems and incorrectly assume specific velocity profile shapes leading to wrong conclusions in the interpretation of data. Another relevant aspect in system flow design is the fact that some flows of Newtonian fluids in microchannels exhibit slip velocity at the walls, specially if they are hydrophobic, as shown in several experimental [1–5] and numerical [6] investigations. A detailed review of experiments on Newtonian fluids showing the existence of slip velocity is given by Neto et al. [7]. Correlations to predict the development length for Newtonian fluid flows, as a function of the Reynolds number and under no-slip boundary conditions, are available in the literature. Recent accurate correlations [8–10] indicate that the development length varies nonlinearly with the Reynolds number, while experimental data of flows in microchannels with a rectangular cross section at low Reynolds numbers [11] showed shorter developing lengths compared to conventional correlations for 2D channel flows. To the best of our knowledge, there is no literature on development lengths for Newtonian fluids in the presence of wall slip. The inclusion of slip boundary conditions in the modeling process is very important, mainly due to the emergence of industrial micro- and nanotechnologies using Newtonian fluids that exhibit wall slip [7,12]. This justifies the present contribution, where a numerical study is presented on the required development lengths for Newtonian fluid flow in planar channels under the influence of slip boundary conditions using the linear Navier slip law [13], with the dimensionless slip coefficient $\overline{k}_l$ varying in the range $0 < \overline{k}_l \leq 1$ ($\overline{k}_l = 1$ corresponds to a significant slip close to a plug velocity profile, and these high slip lengths can be found in experimental results due to the presence of gaseous material at the interface [7]).

2 Equations, Numerical Analysis, and Geometry

It is assumed that this internal flow is two-dimensional, incompressible, laminar, isothermal, and steady. The governing equations for such flow conditions are the continuity

$$\nabla \cdot \mathbf{u} = 0 \tag{1}$$

and the momentum

$$\rho\left(\frac{\partial \mathbf{u}}{\partial t} + \mathbf{u} \cdot \nabla \mathbf{u}\right) = -\nabla p + \nabla \cdot \boldsymbol{\tau} \tag{2}$$

equations, where $\mathbf{u}$ is the velocity vector, p is the pressure, ρ is the fluid density, and $\boldsymbol{\tau}$ is the Newtonian extra-stress tensor, which is given by

$$\boldsymbol{\tau} = \mu\left(\nabla \mathbf{u} + (\nabla \mathbf{u})^T\right) = 2\mu \mathbf{D} \tag{3}$$

where $\mathbf{D}$ is the symmetric rate of deformation tensor and μ is the dynamic viscosity.

The channel geometry and Cartesian coordinate system are represented in Fig. 1. A uniform velocity profile, U, is imposed at the inlet of the planar channel, with all other variables set to zero. Vanishing streamwise gradients are applied to all variables at the outlet plane, except for the pressure, which is linearly extrapolated to the outlet from the two nearest upstream cells. At the wall, the usual no-slip boundary condition was replaced by a wall slip law, in this case, the linear Navier slip law [13],

$$\bar{u}_{ws} = -\bar{k}_l \bar{\tau}_{xy,w} \tag{4}$$

where $\overline{u}_{ws} = u_{ws}/U$ is the dimensionless slip velocity, $\overline{k}_l$ is the dimensionless slip coefficient that allows one to control the

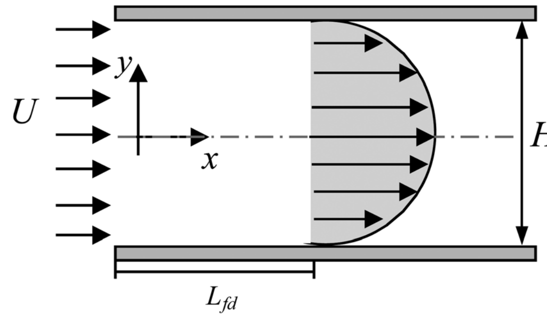

Fig. 1 Schematic representation of the geometry

Table 1 Mesh characteristics

		NC	$\Delta x_{\min}/H$	$\Delta y_{\min}/H$
$L = 10H$	M1	100×40	3.8×10^{-3}	1.2×10^{-3}
	M2	200×80	1.9×10^{-3}	6.2×10^{-4}
	M3	400×160	9.6×10^{-4}	3.1×10^{-4}

intensity of the slip velocity, and $\bar{\tau}_{xy,w} = \tau_{xy,w}(H/U\mu)$ stands for the dimensionless wall shear stress. Equation (4) states that the tangent velocity vector points in the tangent shear stress opposite direction, both variables calculated at the wall. Hence, the Navier slip boundary condition can be written as $\bar{u}_{ws} = \mp \bar{k}_l \mathrm{d}\bar{u}/\mathrm{d}\bar{y}$ (with $\bar{y} = y/H$ and $\bar{u} = u/U$), where the signs (–) and (+) are used for the upper and lower walls, respectively.

The system of Eqs. (1)–(3) is solved by the finite volume method using the SIMPLE procedure of Patankar [14] to couple velocity and pressure fields [15]. The inclusion of slip boundary conditions changes the overall procedure, as explained in detail in Ferrás et al. [16]. With their semi-implicit method, on the verge of convergence, the calculated slip velocity converges to the correct slip velocity, and when it is far from the solution, this new procedure guarantees that the slip velocity is always smaller than the velocity at the center of the adjacent control volume (divergence of the numerical method occurs when this necessary condition is not verified); therefore, there is no need to use direct relaxation in the slip velocity and the computations are stable.

In order to achieve accurate mesh-independent results, the physical domain depicted in Fig. 1 was discretized into three meshes with increasing mesh refinement by doubling the number of cells in the streamwise and transverse directions. Due to symmetry, only half of the domain was used in the numerical simulations. A nonuniform distribution of the cell sizes was used, with the ratio of the geometric progression of the cell sizes in the streamwise direction being 1.05 and 1.01 for the coarse and refined meshes, respectively. For the transverse direction, the cells were concentrated near the channel wall and at the centerplane region to quantify accurately the streamwise variation of the velocity to define well the fully developed flow length. For details about the meshes used in the numerical calculations, see Table 1. The present mesh refinement strategy was designed to provide a detailed and accurate measure of uncertainty in our simulations by using the Richardson extrapolation to the limit technique [17]. This method allows the estimation of the order of accuracy of the simulations (an overall second order was attained in the mesh convergence studies) and an accurate mesh-independent extrapolated $\mathcal{L}_{ext}$ value. More details on this can be found in Table 2, where we provide the results obtained for three specific Reynolds numbers of 0.001, 5, and 100 and four different slip friction coefficients (the "% error" in the table is a quantification of the relative difference between the predictions of $\mathcal{L}$ on the finest mesh (M3) and the extrapolated results ($\mathcal{L}_{ext}$) obtained from Richardson's extrapolation technique).

Table 2 Development length and estimated error for the three different meshes

	Re	M1	M2	M3	$\mathcal{L}_{ext}$	% error
$\bar{k}_l = 0.0001$	0.001	0.6394	0.6308	0.6289	0.6284	0.08
	5	0.7160	0.7007	0.6958	0.6934	0.34
	100	4.9945	4.7927	4.7252	4.6912	0.73
$\bar{k}_l = 0.001$	0.001	0.6402	0.6316	0.6298	0.6293	0.08
	5	0.7171	0.7018	0.6969	0.6945	0.34
	100	4.9986	4.7971	4.7296	4.6955	0.72
$\bar{k}_l = 0.01$	0.001	0.6483	0.6397	0.6381	0.6377	0.06
	5	0.7283	0.7132	0.7085	0.7065	0.29
	100	5.0468	4.8484	4.7814	4.7474	0.72
$\bar{k}_l = 0.1$	0.001	0.6893	0.6832	0.6819	0.6816	0.05
	5	0.8004	0.7873	0.7831	0.7811	0.25
	100	5.5846	5.4168	5.3546	5.3179	0.69
$\bar{k}_l = 1$	0.001	0.5568	0.5560	0.5561	—	—
	5	0.6856	0.6818	0.6806	0.6799	0.10
	100	4.9682	4.9347	4.9235	4.9180	0.11

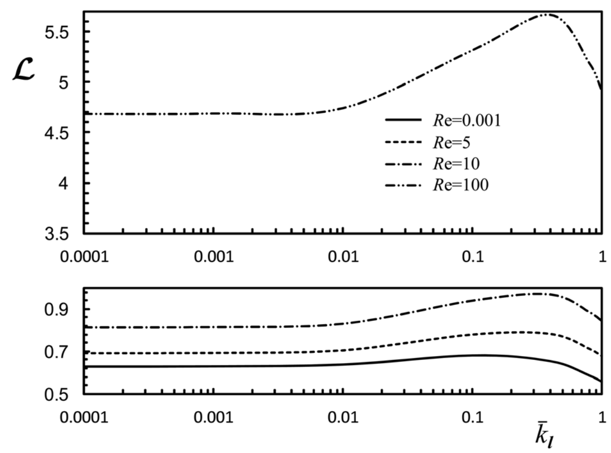

Fig. 2 Variation of the development length ($\mathcal{L}$) with the slip coefficient ($\bar{k}_l$) for three different values of *Re*

3 Results and Discussion

The results obtained show that the development length varies nonmonotonically with the slip coefficient, as observed in Fig. 2. The development length increases at low dimensionless slip coefficients and decreases at high values of $\bar{k}_l$. For $Re = 10^{-3}$, the peak development length occurs for $\bar{k}_l = 0.1$. The development length, $\mathcal{L}$, is here defined as the length from the inlet required for the velocity in the center plane to attain a value of 99% of the corresponding fully developed value and the Reynolds number is defined as $Re = \rho UH/\mu$. As shown in Table 2 and Fig. 2, for creeping flow conditions ($Re = 10^{-3}$) and $\bar{k}_l = 0.1$, an asymptotic limit of $\mathcal{L}_{ext|Re\to 0} = 0.682$ was obtained, while for the no-slip boundary condition, the corresponding asymptotic limit is $\mathcal{L}_{ext|Re\to 0} = 0.628$, as show in Table 3 (which is in agreement with Durst et al. [8]). For the same inertialess conditions and higher values of $\bar{k}_l$, the asymptotic limit decreases, with $\mathcal{L}_{ext|Re\to 0} = 0.556$ at $\bar{k}_l = 1$. Regarding the comparison between the development lengths for the no-slip and the slip cases, we could find differences of the order of 15% for high slip coefficients and below 3% for small slip coefficients. These differences increase with Reynolds number and slip coefficient, as seen in Table 3 and Fig. 3. For small dimensionless slip coefficients and small Reynolds number ($Re \le 10$), these differences are less pronounced.

We propose a correlation (Fig. 4), which is able to predict the development length of Newtonian fluid flows under slip

Table 3 Development length ($\mathcal{L}$) obtained for different values of the slip coefficient ($\bar{k}_l$) and different Reynolds numbers (Re) for the mesh M2 (the extrapolated values are in bold)

Re	$\bar{k}_l = 0.0001$	$\bar{k}_l = 0.001$	$\bar{k}_l = 0.01$	$\bar{k}_l = 0.1$	$\bar{k}_l = 0.4$	$\bar{k}_l = 0.8$	$\bar{k}_l = 1$
0.001	**0.6284**	**0.6293**	**0.6377**	**0.6816**	0.6546	0.5860	0.5560
0.002	0.6308	0.6316	0.6397	0.6832	0.6546	0.5860	0.5560
0.005	0.6308	0.6317	0.6398	0.6833	0.6547	0.5861	0.5561
0.01	0.6309	0.6317	0.6398	0.6833	0.6548	0.5862	0.5562
0.02	0.6310	0.6318	0.6399	0.6835	0.6550	0.5864	0.5564
0.05	0.6313	0.6321	0.6403	0.6840	0.6557	0.5870	0.5570
0.1	0.6317	0.6326	0.6408	0.6848	0.6568	0.5881	0.5581
0.2	0.6327	0.6335	0.6419	0.6863	0.6591	0.5903	0.5603
0.5	0.6356	0.6364	0.6452	0.6911	0.6658	0.5970	0.5667
1	0.6411	0.6420	0.6509	0.7000	0.6773	0.6085	0.5779
2	0.6532	0.6541	0.6638	0.7189	0.7020	0.6327	0.6013
5	**0.6934**	**0.6945**	**0.7065**	**0.7811**	0.7881	0.7162	**0.6799**
10	0.8144	0.8159	0.8310	0.9388	0.9680	0.8860	0.8441
20	1.1560	1.1579	1.1779	1.3456	1.4180	1.3003	1.2366
50	2.4968	2.4995	2.5303	2.8361	2.9924	2.7324	2.5888
100	**4.6912**	**4.6955**	**4.7474**	**5.3179**	5.7238	5.2161	**4.9180**

($0 \le \bar{k}_l \le 1$) for the low Reynolds number range studied here $Re \le 100$. The model is inspired on the works of Durst et al. [8] and Barber and Emerson [18] and is given by

$$\mathcal{L}_{\text{slip}} = \frac{1 + 3.15\bar{k}_l^{1.2} + 0.28\bar{k}_l Re^{0.5}}{1 + 3.82\bar{k}_l^{1.5} + 0.018\bar{k}_l Re}\left[0.631^{1.8} + (0.047Re)^{1.8}\right]^{\frac{1}{1.8}} \tag{5}$$

for $0 \le Re \le 100$ and $\bar{k}_l \le 1$.

We quantified the error between the computed and the correlation values as the average of the relative errors (for each slip coefficient and Reynolds number), and an average error below 1% was obtained.

In Fig. 5, we plot the profiles of the dimensionless streamwise velocity component along the axial direction at several transverse positions for two distinct values of the slip coefficient ($\bar{k}_l = 0.0001$ and 0.1). We can observe in both cases that the dimensionless velocity increases as we move towards the symmetry axis ($y = 0$). The conservation of mass, together with the fact that the wall slip velocity increases with the slip coefficient, forces the centerplane velocity to decrease inversely with $\bar{k}_l$. From the inset in Fig. 5, we can also see that the development length for $\bar{k}_l = 0.1$ is longer than the development length for $\bar{k}_l = 0.0001$. For $\bar{k}_l = 0.0001$, the dimensionless axial velocity component presents a pronounced local maximum close to the channel wall that increases as the Reynolds number increases. For higher values of $\bar{k}_l$, we found that the introduction of the slip velocity tends to suppress the appearance of this near-wall velocity overshoot. To better understand this behavior, we also plotted the transverse profiles of the dimensionless streamwise velocity for various positions along the channel, shown in Fig. 6, for creeping flow conditions ($Re = 10^{-3}$) and $Re = 100$. When the contribution from the slip velocity is negligible ($\bar{k}_l = 0.0001$), the development of the axial velocity profiles is not purely convex and shows a local minimum on the symmetry axis and a local maximum near the walls. These overshoots are generated as a result of the abrupt fluid deceleration happening near the wall at the inlet that happens faster than diffusion is able to transport momentum to the centerplane. As slip increases, this deceleration effect is reduced and the local maximum disappears (for the full slip condition, there is no fluid deceleration). A more in-depth description of this velocity overshoot for nonslip conditions is reported in Darbandi and Schneider [19]. Comparing Figs. 6(*a*) and 6(*b*), we can conclude

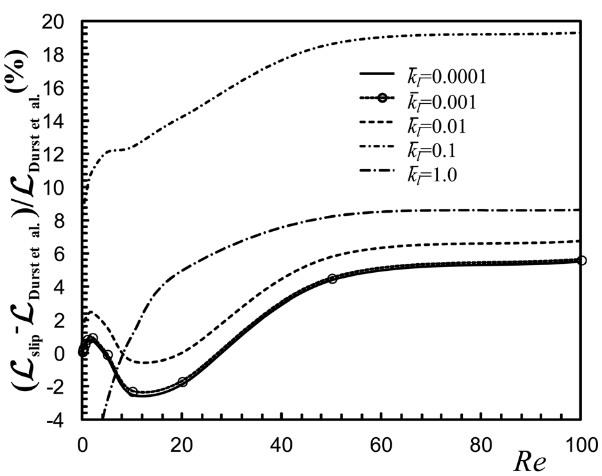

Fig. 3 Variation with *Re* of the difference in $\mathcal{L}$ of Eq. (5) relative to the no-slip case results of Durst et al. [8] as a function of the slip coefficient $\bar{k}_l$

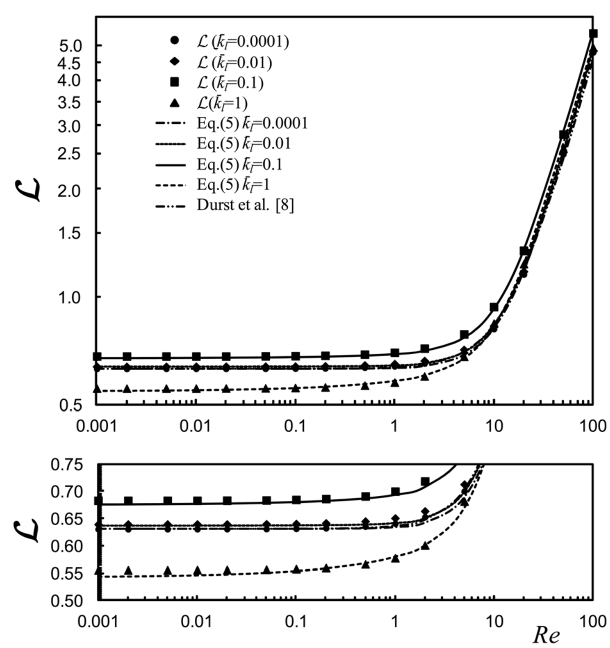

Fig. 4 Nonlinear functional correlations for $\mathcal{L} = f(Re, \bar{k}_l)$ for channel flows

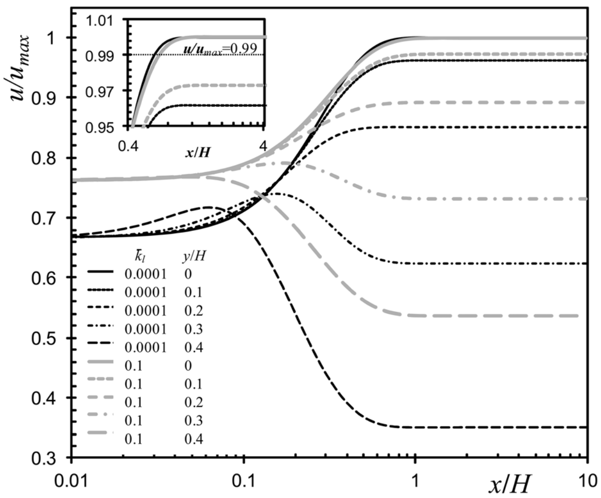

Fig. 5 Dimensionless velocity profiles along the channel for two different values of the slip coefficient ($\bar{k}_l$ = 0.0001 and 0.1) and *Re* = 10^{-3} at five different positions *y/H*. Inset: detailed view near the wall.

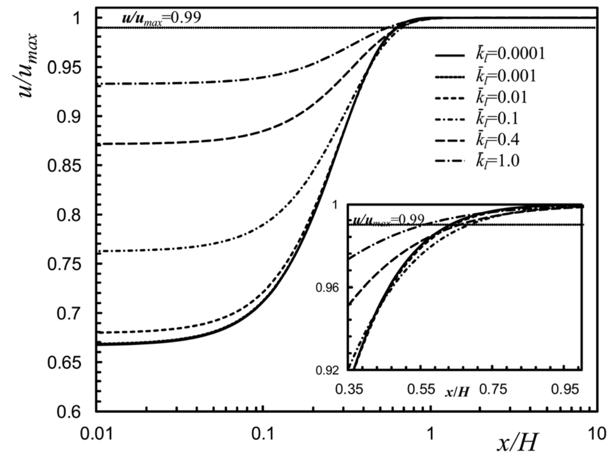

Fig. 7 Variation along the channel of the dimensionless centerplane velocity as a function of the slip coefficient for *Re* = 10^{-3}. Inset: detailed view of the development length for the different slip coefficients.

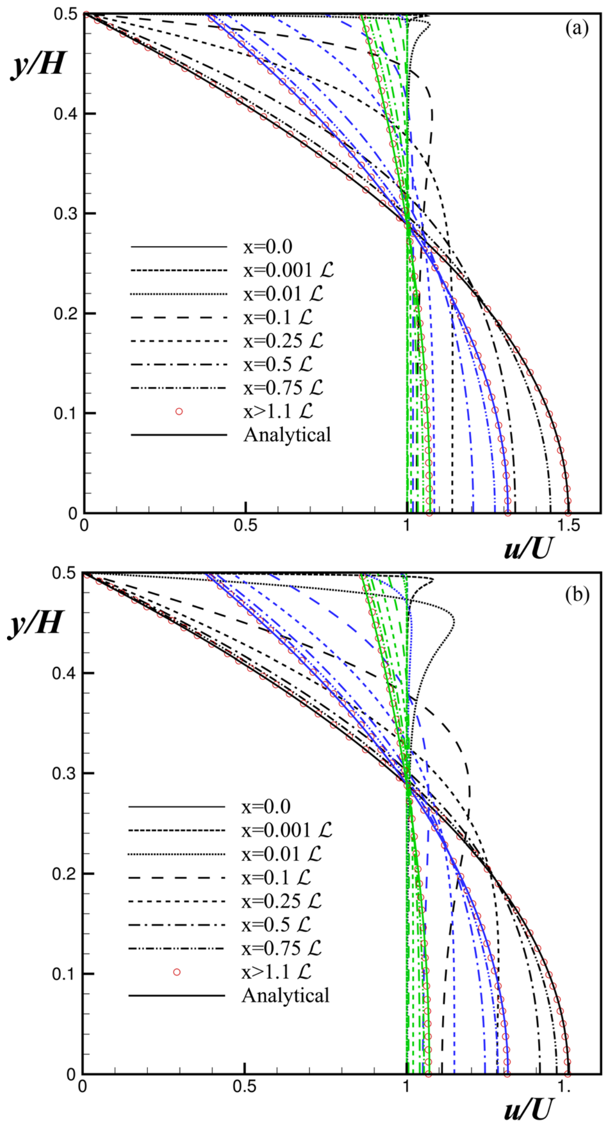

Fig. 6 Velocity profiles at different axial locations for $\bar{k}_l$ = 0.0001 (low slip velocity-black), 0.1 (moderate slip velocity-blue), and 1.0 (high slip velocity-green): (*a*) *Re* = 10^{-3} and (*b*) *Re* = 100

that, for small slip velocities, the overshoots are present, even when inertia is negligible, with their magnitudes (measured by $(u_{y\max} - u_{sa})/u_{sa}$, where $u_{y\max}$ is the local maximum velocity in the profile and u_{sa} is the corresponding velocity at the symmetry axis) increasing with inertia. For all the simulations, the maximum overshoot magnitude is attained for $Re = 100$ with a value of 15.83% (close to 15.8% obtained with $\bar{k}_l = 0$ by Darbandi and Schneider [19]). For higher values of the slip coefficient, the appearance of the velocity overshoots is almost suppressed, as also observed in Figs. 6(*a*) and 6(*b*), where we can see that, for inertialess conditions, there is no overshoot (since *Re* is the ratio between diffusive and advective time scales, the effect of viscosity is transmitted to the whole channel very quickly when $Re = 0$), while for higher Reynolds number ($Re = 100$), a very small overshoot is present only for $\bar{k}_l = 0.1$. This can be explained as a result of a smaller deceleration effect of the fluid elements near the channel walls due to the slip condition, allowing both the convection and diffusion to transport momentum to the centerplane. The velocity at the centerplane is also affected (and indirectly the development length), as observed in the dimensionless velocity profiles along the centerplane for different slip coefficients and $Re \to 0$, plotted in Fig. 7, showing smaller $\mathcal{L}$ for $\bar{k}_l > 0.1$.

4 Conclusions

We conducted a detailed and systematic numerical investigation of the development length in planar channel flows of Newtonian fluids under laminar flow conditions and under the presence of hydrodynamic wall slip. We show that a judicious choice of mesh refinement and highly accurate numerical methods allow the prediction of highly accurate development length values. A new nonlinear correlation for $\mathcal{L}(\bar{k}_l, Re)$ is proposed, which shows good accuracy over the range $\bar{k}_l \le 1$ and $Re \le 100$. This nonlinear correlation predicts a nonmonotonic behavior between the wall slip coefficient and the development length, with the development length increasing up to $\bar{k}_l \approx 0.1$ and $\bar{k}_l \approx 0.4$ for creeping and high inertia ($Re = 100$) flows, respectively, and decreasing for higher values of $\bar{k}_l$.

Acknowledgment

The authors acknowledge funding from COMPETE/FEDER and Fundação para a Ciência e a Tecnologia (FCT), Portugal, through project PTDC/EQU-FTT/113811/2009. L.L.F. would like to thank FCT for financial support through the scholarship SFRH/BD/37586/2007 and A.M.A. through the scholarship SFRH/BPD/75436/2010.

References

[1] Tretheway, D. C., and Meinhart, C. D., 2002, "Apparent Fluid Slip at Hydrophobic Microchannel Walls," Phys. Fluids, **14**, pp. L9–L12.
[2] Watanabe, K., Yanuar, and Mizunuma, H., 1998, "Slip of Newtonian Fluids at Slid Boundary," JSME Int. J., Ser. B, **41**, pp. 525–529.
[3] Watanabe, K., Udagawa, Y., and Udagawa, H., 1999, "Drag Reduction of Newtonian Fluid in a Circular Pipe With a Highly Water-Repellant Wall," J. Fluid Mech., **381**, pp. 225–238.
[4] Zhu, Y., and Granick, S., 2001, "Rate-Dependent Slip of Newtonian Liquid at Smooth Surfaces," Phys. Rev. Lett., **87**, p. 096105.
[5] Ligrani, P., Blanchard, D., and Gale, B., 2010, "Slip Due to Surface Roughness for a Newtonian Liquid in a Viscous Microscale Disk Pump," Phys. Fluids, **22**, p. 052002.
[6] Barrat, J., and Bocquet, L., 1999, "Large Slip Effect at a Nonwetting Fluid-Solid Interface," Phys. Rev. Lett., **82**, pp. 4671–4674.
[7] Neto, C., Evans, D. R., Bonaccurso, E., Butt, H.-J., and Craig, V. S., 2005, "Boundary Slip in Newtonian Liquids: A Review of Experimental Studies," Rep. Prog. Phys., **68**, pp. 2859–2897.
[8] Durst, F., Ray, S., Unsal, B., and Bayoumi, O. A., 2005, "The Development Lengths of Laminar Pipe and Channel Flows," ASME J. Fluids Eng., **127**, pp. 1154–1160.
[9] Poole, R. J., and Ridley, B. S., 2007, "Development-Length Requirements for Fully Developed Laminar Pipe Flow of Inelastic Non-Newtonian Liquids," ASME J. Fluids Eng., **129**, pp. 1281–1287.
[10] Poole, R. J., and Chhabra, R. P., 2010, "Development Length Requirements for Fully Developed Laminar Pipe Flow of Yield Stress Fluids," ASME J. Fluids Eng., **132**, p. 034501.
[11] Lee, S. Y., Jang, J., and Wereley, S. T., 2008, "Effects of Planar Inlet Plenums on the Hydrodynamically Developing Flows in Rectangular Microchannels of Complementary Aspect Ratios", Microfluidics Nanofluidics, **5**(1), pp. 1–12.
[12] Lauga, E., Brenner, M. P., and Stone, H. A., 2007, *Handbook of Experimental Fluid Dynamics*, C. Tropea, A. Yarin, and J. F. Foss, eds., Springer, New York, pp. 1219–1240, Chap. 19.
[13] Navier, C. L. M. H., 1827, "Sur les Lois du Mouvement des Fluids," Mem. Acad. R. Sci. Inst. Fr., **6**, pp. 389–440.
[14] Patankar, S. V., 1980, *Numerical Heat Transfer and Fluid Flow*, Hemisphere, Washington, D.C.
[15] Oliveira, P. J., Pinho, F. T., and Pinto, G. A., 1998, "Numerical Simulation of Non-Linear Elastic Flows With a General Collocated Finite-Volume Method," J. Non-Newtonian Fluid Mech., **79**, pp. 1–43.
[16] Ferrás, L. L., Nóbrega, J. M., and Pinho, F. T., "Implementation of Slip Boundary Conditions in the Finite Volume Method: New Techniques," Int. J. Numer. Methods Eng. (submitted).
[17] Richardson, L. F., 1911, "The Approximate Arithmetical Solution by Finite Differences of Physical Problems Involving Differential Equations, With an Application to the Stresses in a Masonry Dam," Philos. Trans. R. Soc. London, Ser. A, **210**, pp. 307–357.
[18] Barber, R. W., and Emerson, D. R., 2001, "A Numerical Investigation of Low Reynolds Number Gaseous Slip Flow at the Entrance of Circular and Parallel Plate Micro-Channels", Proc. ECCOMAS Computational Fluid Dynamics Conference 2001.
[19] Darbandi, M., and Schneider, G. E., 1998, "Numerical Study of the Flow Behavior in the Uniform Velocity Entry Flow Problem," Numer. Heat Transfer, Part A, **34**(5), pp. 479–494.